Author/s:
Hudson, RJ;Manian, A;Hall, CR;Schmidt, TW;Russo, SP;Ghiggino, KP;Smith, TA

Title:
Quantifying the Relaxation Dynamics of Higher Electronic Excited States in Perylene.

Date:
2023-08-31

Citation:
Hudson, R. J., Manian, A., Hall, C. R., Schmidt, T. W., Russo, S. P., Ghiggino, K. P. & Smith, T. A. (2023). Quantifying the Relaxation Dynamics of Higher Electronic Excited States in Perylene.. Journal of Physical Chemistry Letters, 14 (36), pp.8000-8008. https://doi.org/10.1021/acs.jpclett.3c02071.

Persistent Link:
https://hdl.handle.net/11343/337167

Quantifying the Relaxation Dynamics of Higher Electronic Excited States in Perylene

Rohan J. Hudson,[*,†,§] Anjay Manian,[‡,§] Christopher R. Hall,[†,§] Timothy W. Schmidt,[¶,§] Salvy P. Russo,[‡,§] Kenneth P. Ghiggino,[†,§] and Trevor A. Smith[*,†,§]

†*School of Chemistry, The University of Melbourne, Parkville, 3010, VIC, Australia*

‡*School of Science, RMIT University, Melbourne, 3000, VIC, Australia*

¶*School of Chemistry, The University of New South Wales, Sydney, 2052, NSW, Australia*

§*Australian Research Council Centre of Excellence in Exciton Science*

E-mail: rohan.hudson@unimelb.edu.au; trevoras@unimelb.edu.au

Phone: +61 3 8344 6272. Fax: +61 3 9347 5180

Abstract

Gating logical operations through high-lying electronic excited states presents opportunities for developing ultrafast, sub-nanometer computational devices. A lack of molecular systems with sufficiently long-lived higher excited states has hindered practical realisation of such devices, but recent studies have reported intriguing photophysics from high-lying excited states of perylene. In this work, we use femtosecond spectroscopy supported by quantum chemical calculations to identify and quantify relaxation dynamics of monomeric perylene's higher electronic excited states. The 2^1B_{2u} state is accessed through single-photon absorption at 250 nm, while the optically-dark 2^1A_g state is excited via the 1^1B_{3u} state. Population of either state results in sub-picosecond relaxation to the 1^1B_{3u} state, and we quantify 2^1A_g and 2^1B_{2u} state lifetimes of 340 fs and 530 fs, respectively. These lifetimes are significantly longer than the singlet fission time constant from the perylene 2^1B_{2u} state, suggesting that perylene's higher electronic states may be useful for gating logical operations.

TOC Graphic

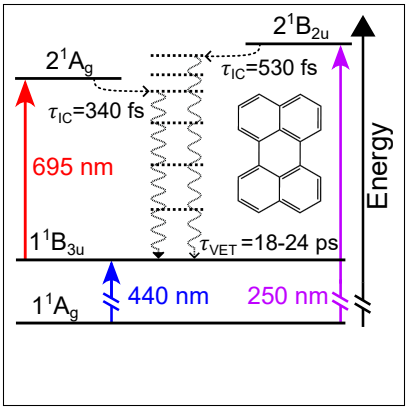

Keywords

Femtosecond Spectroscopy, Pump-Push-Probe Spectroscopy, Perylene, Higher Excited States, Internal Conversion

The field of molecular logic, whereby single molecules conduct logical operations for information processing purposes, has expanded significantly in recent years.[1,2] Performing logical operations with discrete molecular systems is highly desirable as it could allow for the construction of sub-nanometer circuit components.[3,4] Light is an ideal input/output interface for molecular logic, as optical signals can be spectrally tuned and spatially targeted at specific molecular components and can facilitate signal processing orders of magnitude faster than inputs reliant upon chemical diffusion. Early demonstrations of molecular logic gates modulated local ionic environments to turn on or off molecular photoluminescence.[5–7] More recent reports use optical inputs and outputs by employing photoswitchable chromophores,[1] however the slow timescale of photoisomerisation (ensemble switching lifetimes on the order of seconds–minutes[8–10]) fundamentally restricts the processing throughput of any such molecular logic devices in most practical applications.

An alternative implementation of an all-optical molecular logic system is to gate logical operations through high-lying electronic excited states.[11,12] Such a system would permit the use of optical input and output signals without requiring any molecular rearrangement through photoswitching, facilitating ultrafast signal processing on a sub-nanosecond scale. Such a molecular logic device is difficult to practically realise, however, as very few molecules possess sufficiently long-lived higher electronic excited states. Excitation to such high-lying states in most compounds generally results in ultrafast relaxation to the lowest electronic excited state, in accordance with Kasha's Rule.[13] Exceptions to this of course exist; azulene and its derivatives exhibit S_2 fluorescence lifetimes on the order of nanoseconds.[14–16] Previous studies of a bichromophoric azulene-rhodamine dyad demonstrated the potential to operate a "full adder" logic device by gating operations through the multiple optically-active excited states of azulene.[17,18] However, the efficiency of these devices was limited by the relatively short-lived azulene S_1 state, which decays on a sub-picosecond scale due to a conical intersection with the ground state.[19,20] While certain azulene-based derivatives do exhibit longer S_1 lifetimes than azulene itself,[21] the viability of employing these compounds in molecular

logic systems has yet to be established. Further development of this form of molecular logic therefore requires investigation into appropriate chromophores with sufficiently long-lived higher excited states.

One candidate molecule for gating logical operations through high-lying excited states is the fused polyaromatic hydrocarbon perylene (Figure 1). Singlet fission (SF), a photophysical process whereby a singlet exciton converts into a pair of triplet excitons, has been reported to occur from electronic excited states in perylene higher in energy than the S_1 state.[22,23] SF from the lowest-energy singlet excited state in crystalline perylene is highly endoergic and is hence not observed upon low-energy excitation,[24,25] but high-energy excitation has been demonstrated to form triplet excitons on a sub-picosecond timescale.[22,23,26] Gating SF through high-lying excited states would be highly desirable from a molecular logic perspective, as the distinctly different magneto-optical properties of singlet and triplet excitons could facilitate ultrafast information processing with readily-distinguishable on/off signals. However, the precise details of the higher-excited state processes associated with SF in perylene are not yet fully understood. Conflicting reports have emerged regarding whether SF occurs directly from a high-lying electronic excited state or a vibrationally-hot S_1 state following internal conversion.[26–28] Assignment of the high-lying electronic excited states in perylene has also been ambiguous and inconsistent within the literature: several studies have attributed perylene's strong ultraviolet absorption at $\sim$250 nm to the $S_2 \leftarrow S_0$ transition,[23,26,27,29] despite this being symmetry-forbidden and predicted to occur at around 350 nm.[30] A clearer understanding of the identities and dynamics of perylene's high-lying electronic excited states is therefore necessary for any potential development of molecular logic circuits involving perylene.

In this work, we use transient absorption (TA) spectroscopy and a combination of quantum chemical *ab initio* methods to investigate the electronic excited states of monomeric perylene accessible through UV-visible excitation. We study the photophysics of perylene in dilute solution to minimize the influence of multichromophoric processes such as excimer

formation or singlet fission, such that the nature and behavior of perylene's higher electronic excited states can be unambiguously characterized. Two excited states can be populated via direct transitions from the ground state: the 1^1B_{3u} state at 2.82 eV and the 2^1B_{2u} state at 4.96 eV. A strong excited-state absorption (ESA) is observed at 695 nm, which is assigned as the $2^1A_g \leftarrow 1^1B_{3u}$ transition. Using pump-push-probe spectroscopy, $2^1A_g \rightarrow 1^1B_{3u}$ internal conversion (IC) is observed to occur over 340 fs, followed by vibrational cooling within the 1^1B_{3u} manifold over tens of picoseconds. Relaxation from the 2^1B_{2u} state is slightly slower than this, with a lifetime of 530 fs measured here. These IC rates from high-lying excited states are both an order of magnitude slower than previously-reported rates of SF in condensed-phase perylene, thus suggesting that SF could proceed from perylene's high-lying states upon either one- or two-pulse excitation.

Steady-state absorption and emission spectra of perylene in cyclohexane solution are shown in Figure 1. Major spectral features are labelled alphabetically to simplify discussion and identification. The lowest-energy absorption feature is a vibronic band from 350–440 nm (Figure 1*a*), corresponding to the well-characterised $S_1 \leftarrow S_0$ electronic transition in perylene.[31–35] The steady-state emission from 440–550 nm is a clear mirror image of this absorption band with a minimal Stokes shift (Figure 1*a*′), and is hence assigned to the radiative $S_1 \rightarrow S_0$ transition. Previous studies have reported a quantum yield of close to unity for this emission band,[31–34] thus demonstrating that radiative decay is the dominant relaxation mechanism from the perylene S_1 state. Two higher-energy absorption bands are also observable in the steady-state absorption spectrum of perylene: a very weak feature at 295 nm (Figure 1*b*), and a strong absorption centered at 250 nm (Figure 1*c*).

To identify the electronic excited states involved in these transitions, we performed TDDFT calculations upon monomeric perylene at the B3LYP/aug-cc-pVTZ level of theory. Table 1 lists all singlet excited states of perylene calculated to lie within 5 eV of the ground state (see Sections S1 & S2 of the Supporting Information for further details). The ground electronic state of perylene has A_g symmetry, and only three transitions to higher

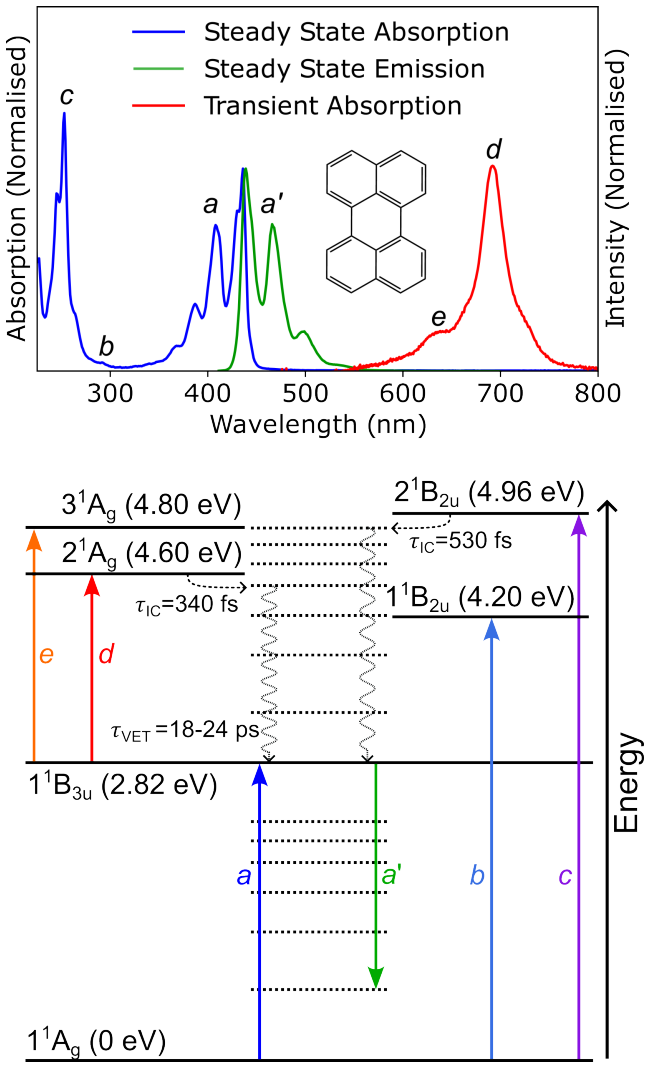

Figure 1: (Top) Normalised steady-state absorption (blue trace; left axis), steady-state emission (green trace, right axis) and transient absorption (red trace, left axis) spectra of perylene/cyclohexane solution. Inset shows the chemical structure of perylene. (Bottom) Jablonski diagram showing the (singlet) excited states of perylene accessible in the UV-visible region through 1- or 2-pulse excitation. Solid horizontal lines denote electronic states; dotted horizontal lines represent vibrational states. Solid arrows represent radiative transitions, with alphabetical labels indicating the spectral features corresponding to these transitions in the spectra presented above. Non-radiative transitions are indicated by dashed arrows, and are labelled by their corresponding time constants; "IC" and "VET" denote internal conversion and vibrational energy transfer, respectively. All energies are listed relative to the 1^1A_g (ground) electronic state.

Table 1: Calculated (B3LYP/aug-cc-pVTZ theory level) and experimentally observed singlet excited states of perylene.

State	Energy (eV)	μ (a.u.)*	Observed Energy (eV)**
1^1A_g	0		
1^1B_{3u}	2.84	0.321	2.82 (a)
1^1B_{1g}	3.63		
2^1B_{1g}	3.95		
1^1B_{2u}	4.05	0.007	4.20 (b)
3^1B_{1g}	4.09		
2^1A_g	4.24		$\sim$ 4.60 ($a+d$)
1^1A_u	4.41		
3^1A_g	4.53		$\sim$ 4.80 ($a+e$)
1^1B_{2g}	4.65		
1^1B_{3g}	4.65		
2^1B_{2u}	4.84	0.316	4.96 (c)

* Transition dipole moments calculated from the ground (1^1A_g) state
** Letters in parentheses refer to transitions labelled in Figure 1

excited states are predicted to have non-zero transition dipole moments (TDMs). The 1^1B_{3u} is calculated as the lowest-energy excited state in the singlet manifold, with a predicted transition energy of 2.84 eV agreeing closely with the $S_1 \leftarrow S_0$ band origin observed in Figure 1. Spectral features a and a' can hence be assigned as corresponding to the $1^1B_{3u} \leftrightarrow 1^1A_g$ transitions in perylene. The $1^1B_{2u} \leftarrow 1^1A_g$ transition is calculated to lie at 4.05 eV with a very weak TDM, while the predicted $2^1B_{2u} \leftarrow 1^1A_g$ transition is higher in energy with TDM comparable to the $S_1 \leftarrow S_0$ transition. These descriptions closely match higher-energy absorption bands b and c observed here, with predicted transition energies agreeing with experimental values within 0.15 eV. Absorption features b and c are thus assigned as the $1^1B_{2u} \leftarrow 1^1A_g$ and $2^1B_{2u} \leftarrow 1^1A_g$ transitions, respectively. Several recent studies assigned the 250-nm absorption in perylene as corresponding to the $S_2 \leftarrow S_0$ transition,[18,21,24] however we note that the 2^1B_{2u} state is calculated here as the eleventh excited state in the singlet manifold, agreeing with other previous studies.[30,36,37]

Transient absorption (TA) spectra of perylene/cyclohexane solution upon exciting the $1^1B_{3u} \leftarrow 1^1A_g$ transition at 440 nm are shown in Figure 2a. Three transient spectral features are evident upon excitation: a strong excited-state absorption (ESA) centered at 695 nm

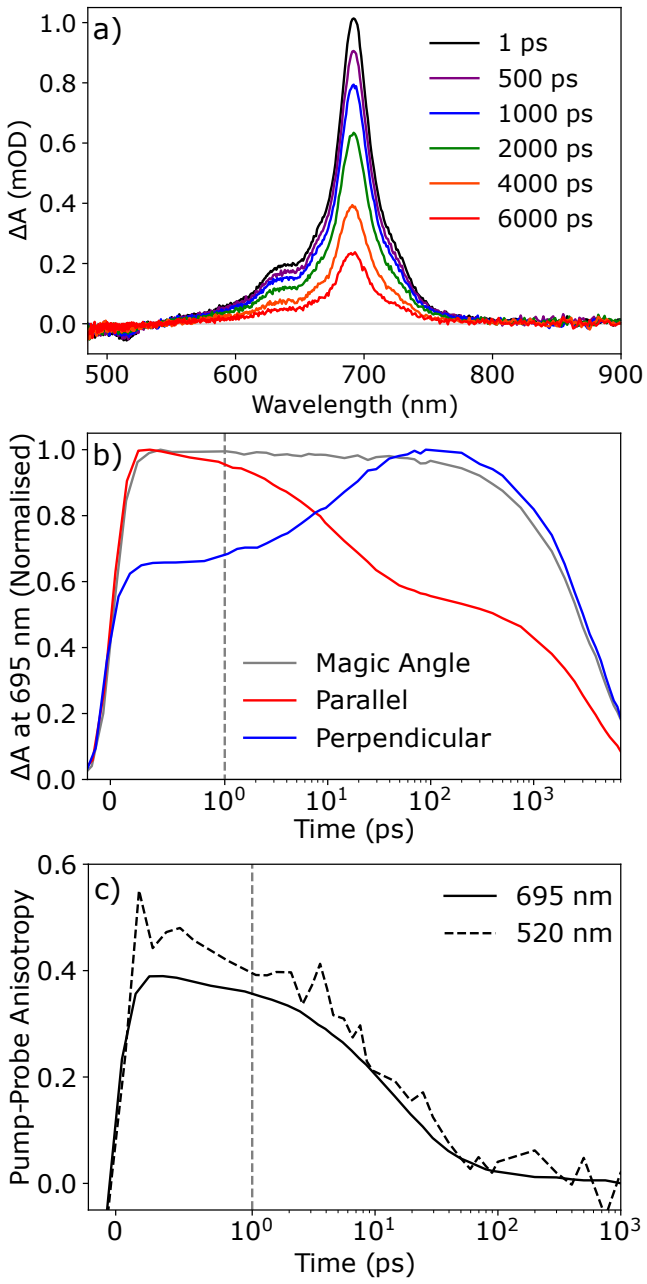

Figure 2: (a) Transient absorption spectra of 100 µM perylene/cyclohexane solution upon excitation at 440 nm with pump and probe relative polarisations at the magic angle (54.7°). (b) Normalised kinetics of the 695-nm ESA at the magic angle, parallel and perpendicular relative pump-probe polarisations. (c) Polarisation anisotropy of the 695-nm ESA and the 520-nm SE transient spectral features. Vertical dashed lines in b & c indicate a crossover from linear to logarithmic scales on the time axis.

(Figure 1*d*), a weaker ESA at 625 nm (Figure 1*e*), and a weak negative-going feature at 500–525 nm due to stimulated emission (SE). All three of these transient spectral features relax monoexponentially with no change in spectral shape on a timescale consistent with the fluorescence lifetime of perylene (Supporting Information, Section S3), and so we assign these as electronic transitions arising from the 1^1B_{3u} state. Other time-resolved studies of perylene have also reported picosecond- and sub-picosecond relaxation components in a variety of solvents upon excitation at wavelengths below 440 nm, ascribed to intramolecular vibrational redistribution within the 1^1B_{3u} manifold.[29,38,39] This is not observed here as the 440-nm pump pulse excites the lowest energy vibronic band within the $1^1B_{3u} \leftarrow 1^1A_g$ transition, and so there is no excess vibrational energy available for redistribution. The SE at 500–525 nm clearly arises from the $1^1B_{3u} \rightarrow 1^1A_g$ transition, however the exact electronic states associated with ESA bands *d* & *e* required further investigation.

To identify the excited states associated with these ESA features, we performed polarisation-dependent pump-probe experiments. Kinetic traces of the 695-nm ESA at different pump-probe polarisations are shown in Figure 2b. While this spectral feature exhibits a monoexponential relaxation at magic angle polarisation, substantially different dynamics are observed upon varying pump-probe polarisation. For pump and probe polarised parallel to one another, an additional fast relaxation component on the order of 10–20 ps is observed, while for perpendicular polarisations a growth in the signal occurs over a similar timescale. These rapid kinetics at different pump-probe polarisations can be attributed to rotational dynamics of perylene molecules in solution, and are indicative of the 695-nm ESA having a transition dipole moment polarised parallel to that of the $1^1B_{3u} \leftarrow 1^1A_g$ transition. At parallel pump-probe polarisations, perylene molecules excited into the 1^1B_{3u} state quickly rotate out of the plane of polarisation, reducing the apparent ESA intensity as they can no longer interact with the probe pulse. The reverse is true for perpendicular relative polarisations, as excited-state molecules rotate into the plane of probe polarisation and cause a signal growth over time. Biexponential fits to these polarisation-dependent kinetics suggest a rotational

reorientation time of approximately 15 ps (Supporting Information, Section S3), agreeing closely with previous measurements of perylene's rotational dynamics in cyclohexane and n-hexane.[40,41]

To further confirm the orientation of the 695-nm ESA transition dipole moment, we compare the pump-probe anisotropy $r(\lambda, t)$ of the transient signals observed here. $r(\lambda, t)$ is calculated as

$$r(\lambda, t) = \frac{\Delta A_{\parallel}(\lambda, t) - \Delta A_{\perp}(\lambda, t)}{\Delta A_{\parallel}(\lambda, t) + 2\Delta A_{\perp}(\lambda, t)}, \tag{1}$$

where $\parallel$ and $\perp$ subscripts denote parallel and perpendicular pump-probe polarisations, respectively.[42,43] Figure 2c displays pump-probe anisotropy for both the 695-nm ESA and the 520-nm SE signals. These two spectral features exhibit effectively identical polarisation anisotropy profiles beyond the initial instrument response. This similarity in polarisation anisotropy supports the earlier assertion that this ESA has a transition dipole moment oriented parallel to that of the $1^1B_{3u} \leftrightarrow 1^1A_g$ transitions. The strong signal intensity of this ESA also indicates that this is a symmetry-allowed transition, and must therefore exhibit a $u \rightarrow g$ change in parity. The high-lying electronic excited state populated by the 695-nm ESA must hence possess A_g symmetry. Using the adiabatic transition wavelengths of 440 and 695 nm observed here, we estimate that this state lies at an energy of approximately 4.6 eV above the ground state, which is reasonably close to the predicted 2^1A_g energy (Table 1), and agrees with other previous estimates of this state.[30,36,37] Therefore, we assign ESA d at 695 nm as corresponding to the $2^1A_g \leftarrow 1^1B_{3u}$ transition.

ESA band e at 625 nm exhibits identical polarisation-dependent dynamics and pump-probe anisotropy to the stronger $2^1A_g \leftarrow 1^1B_{3u}$ band (Supporting Information, Section S3). It is therefore reasonable to conclude that this ESA also arises from a $n^1A_g \leftarrow 1^1B_{3u}$ transition. This feature may correspond to a higher-order vibronic transition within the $2^1A_g \leftarrow 1^1B_{3u}$ manifold or it may involve a different electronic state such as 3^1A_g; it is difficult to distinguish between these possibilities based solely upon the experimental data presented here. However, TDDFT calculations predict the 3^1A_g state to lie approximately 0.3 eV

above the 2^1A_g (Table 1), agreeing relatively closely with the observed energy difference between ESA bands *d* and *e* ($\sim$ 0.2 eV). This suggests that ESA *e* may correspond to the $3^1A_g \leftarrow 1^1B_{3u}$ transition, and so to investigate this we performed complete active space self-consistent field (CASSCF) calculations to characterize which higher electronic states of perylene are strongly coupled to the 1^1B_{3u} state (details of these calculations are presented in the Supporting Information, Sections S1 and S2). These CASSCF calculations indicate that the 2^1A_g and 3^1A_g states both exhibit significant couplings to the 1^1B_{3u} state, with the $3^1A_g \leftarrow 1^1B_{3u}$ TDM slightly weaker than that of $2^1A_g \leftarrow 1^1B_{3u}$. Aided by TDDFT and CASSCF calculations, we therefore assign ESA band *e* at 625 nm as arising from the $3^1A_g \leftarrow 1^1B_{3u}$ transition in perylene.

The 2^1A_g and 3^1A_g states are optically dark from the ground state and thus inaccessible through single-photon excitation. However, the strong $2^1A_g \leftarrow 1^1B_{3u}$ ESA observed here suggests that sequential two-pulse excitation may be a viable pathway for accessing this high-lying electronic excited state. To investigate this, we performed pump-push-probe measurements on perylene/cyclohexane solution, pumping the $1^1B_{3u} \leftarrow 1^1A_g$ transition at 440 nm and then further exciting with a 695-nm "push" pulse resonant with the $2^1A_g \leftarrow 1^1B_{3u}$ transition. The push pulse was timed to arrive 1.1 ps after the pump pulse, and TA spectra at representative delay times before and after the arrival of the push are shown in Figure 3a. Immediately after arrival of the push pulse, the SE and ESA features are reduced in intensity as the push pulse depopulates some of the 1^1B_{3u} state from which these transitions arise. A slight recovery in these signals is then observed over hundreds of femtoseconds, accompanied by a broadening and redshift of the ESA bands. This broadening and reduction of ESA intensity persists for tens of picoseconds, eventually recovering to the original pump-probe signal more than 50 ps after arrival of the push pulse (Figure 3b).

To isolate the spectral dynamics observed due to excitation to the high-lying 2^1A_g state here, we performed additional experiments to measure the change in ΔA due to the push

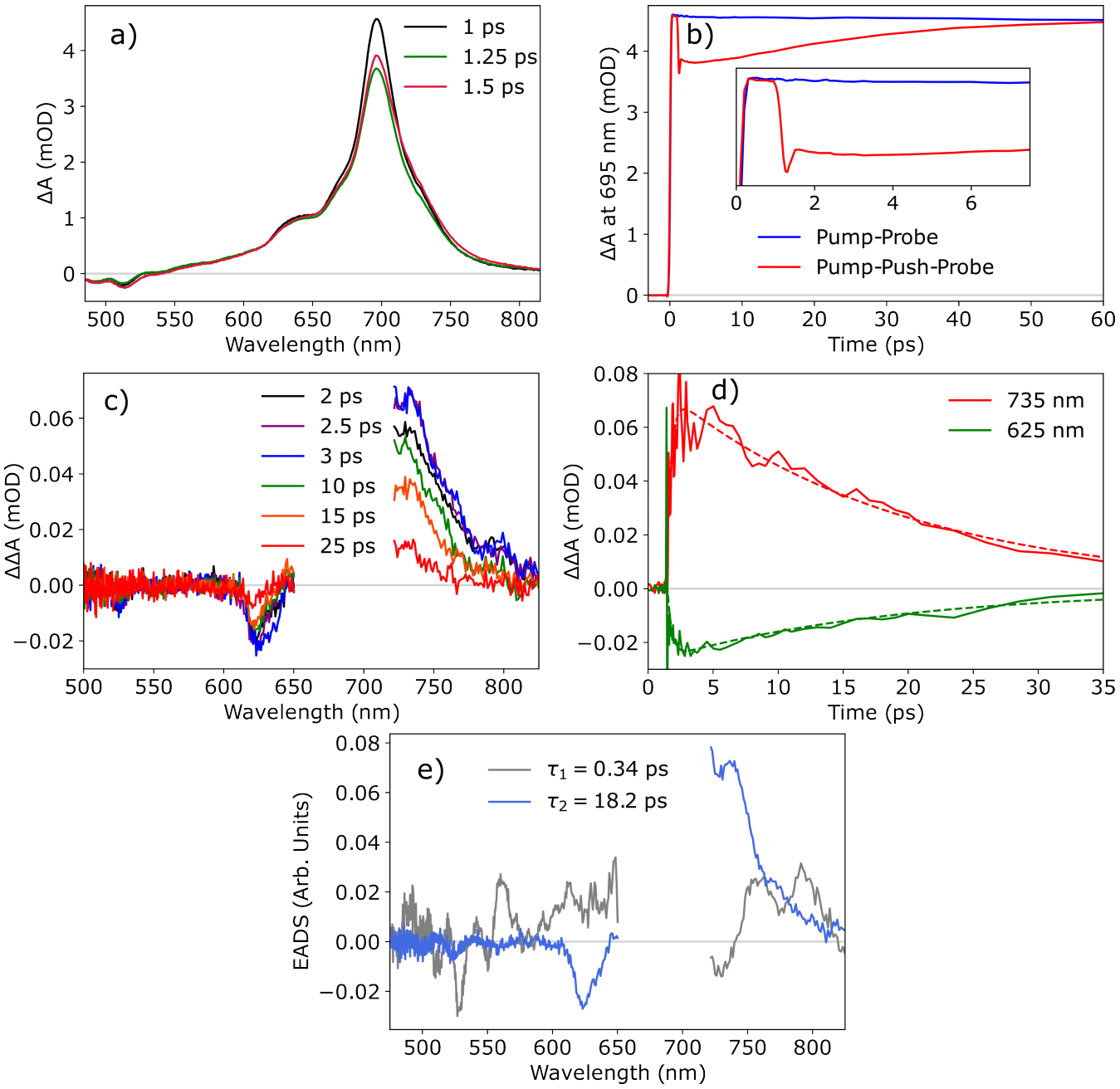

Figure 3: (a) Transient absorption spectra of 100 µM perylene/cyclohexane upon excitation at 440 nm, at representative delay times immediately before and after the arrival of 695-nm push pulse 1.1 ps after the pump. (b) Single-wavelength kinetic profile of the 695-nm ESA for pump-probe and pump-push-probe experiments. Inset shows the change in ΔA at early times due to the push pulse. (c) ΔΔA transient spectra due to the push pulse, at a range of representative delay times. (d) Single-wavelength kinetics of the ΔΔA transient at spectral regions of interest. Dashed lines show fits from global analysis. (e) Evolution-associated difference spectra (EADS) from a global fit to the ΔΔA data with a two-component sequential model. Spectral components are labelled by their characteristic time constants. All delay times are listed relative to pump-probe overlap.

pulse; a $\Delta\Delta$A signal. This quantity is defined as

$$\Delta\Delta\mathrm{A}(\lambda, t) = \Delta\mathrm{A}(\lambda, t)_{\text{Push On}} - \Delta\mathrm{A}(\lambda, t)_{\text{Push Off}}, \tag{2}$$

and was measured by modulating the push pulse while operating both pump and probe at 50 kHz. The 695-nm push pulse used here was not resonant with any ground state absorption features of perylene, and so no push-probe signal was observed in the absence of the pump pulse (Supporting Information, Section S4). Two-photon excitation of the perylene ground state by the push pulse was also not observed, as the frequency-doubled push energy does not overlap with any ground state absorption peaks (see Figure 1). Therefore, we are confident in assigning the $\Delta\Delta$A signals observed in this experimental configuration as arising from two-pulse excitation to the perylene $2^1\mathrm{A_g}$ state.

$\Delta\Delta$A spectra at representative delay times after arrival of the push pulse are shown in Figure 3c (all delay times are listed relative to pump-probe overlap). Within 1 ps of push arrival, bleach signals are evident at 525 and 625 nm, corresponding to the decrease in ΔA intensity at these wavelengths as observed above. Note that data in the spectral range of 650–720 nm have been excluded here due to scatter of the push pulse overwhelming the $\Delta\Delta$A signal in this region, and so no bleach at 695 nm is observed in this experiment. However, the $\Delta\Delta$A spectrum is dominated by a positive feature from 720–800 nm, corresponding to the broadening and redshift of the 695-nm ESA noted above. All of these $\Delta\Delta$A signals exhibit a weak growth over hundreds of femtoseconds after push-probe overlap, before decaying on a timescale of tens of picoseconds (illustrated in Figure 3d).

The broadening and red-shift in the 695-nm ESA observed after arrival of the push pulse (and corresponding positive $\Delta\Delta$A signal from 720–800 nm) is likely due to the population of higher vibrational excited states within the $1^1\mathrm{B_{3u}}$ manifold, reducing the $2^1\mathrm{A_g} \leftarrow 1^1\mathrm{B_{3u}}$ transition energy and broadening the distribution of possible transition energies. We therefore propose that the dominant $\Delta\Delta$A signal observed here corresponds to a vibrationally-hot

1^1B_{3u} state, growing on a sub-picosecond timescale due to $2^1A_g \rightarrow 1^1B_{3u}$ IC and then decaying over tens of picoseconds through vibrational relaxation within the 1^1B_{3u} manifold. In dilute solution such vibrational cooling is expected to occur primarily through solvent-solute vibrational energy transfer (VET), and so would be influenced by the nature of the solvent.[38–40,44] To test our hypothesis of the ΔΔA signal relaxation occurring through VET, we repeated these pump-push-probe experiments with perylene dissolved in toluene. The rate of both short-range (collisional) and longer-range (resonant) VET depends upon the difference in energy between donor and acceptor vibrational modes.[44] The aromatic core of toluene possesses vibrational modes which are more closely aligned with those of perylene than the aliphatic cyclohexane ring, and so we would expect VET for perylene to be faster in toluene solution than in cyclohexane. The perylene ΔΔA transient signal does indeed relax significantly faster in toluene than in cyclohexane solution (Supporting Information, Section S5), thus supporting our assignment of vibrational cooling within the 1^1B_{3u} state causing this ps-scale signal decay.

To quantify these rates of IC and VET observed upon pushing perylene into the 2^1A_g state, we performed a global analysis of the ΔΔA spectra using the Glotaran software package.[45] The minimal model required to adequately describe the data was a two-component sequential scheme, with evolution-associated difference spectra (EADS) of these components shown in Figure 3e. The first component ($\tau_1 = 340\,\text{fs}$) corresponds to the sub-picosecond growth observed in the ΔΔA signal, with broad positive features from 550–650 nm and 750–825 nm. Some oscillatory structure is also present in this EADS due to contamination from coherent artefacts in the signal arising from push-probe overlap. Despite these oscillatory features, however, this component fits well with the observed rise in the ΔΔA signal, and so we are confident that the value of τ_1 extracted here is acceptably accurate despite this spectral contamination. The second spectral component identified by global analysis ($\tau_2 = 18.2\,\text{ps}$) exhibits all of the spectral features discussed above as corresponding to a vibrationally-hot 1^1B_{3u} state, and so we assign this component as arising from vibrational

cooling in the 1^1B_{3u} manifold through VET. Given that the push pulse initially populates the perylene 2^1A_g state, the first component must therefore correspond to $2^1A_g \rightarrow 1^1B_{3u}$ relaxation. We hence assign this first $\Delta\Delta A$ spectral component as $2^1A_g \rightarrow 1^1B_{3u}$ IC, with a 2^1A_g lifetime of approximately 340 fs.

The 2^1A_g state is not the only high-lying state of perylene accessible through optical excitation (Figure 1); the 2^1B_{2u} state may also be populated directly from the ground state through excitation in the UV. To study the relaxation dynamics of the 2^1B_{2u} state, we also performed pump-probe experiments on perylene solution at an excitation wavelength of 270 nm, resonant with the low-energy edge of the $2^1B_{2u} \leftarrow 1^1A_g$ transition. Figure 4a shows the resulting TA spectra, which are substantially different to those obtained from 440-nm excitation. Immediately after excitation two ESA bands are again observed, but significantly broadened and redshifted relative to those shown in Figure 2. These features exhibit a growth over the initial 2 ps after excitation, before then blueshifting, narrowing and further increasing in intensity on a timescale of tens of picoseconds (Figure 4b). After 50 ps, the TA spectra resemble those obtained upon excitation of the $1^1B_{3u} \leftarrow 1^1A_g$ transition at 440 nm, and decay over several nanoseconds.

We thus observe three distinct timescales of spectral evolution upon excitation at 270 nm, and so to identify and quantify the physical processes underpinning these we again interrogated the TA spectra using global analysis. A three-component sequential model was found to be the minimal representation required to adequately describe the data, and EADS from this fit are shown in Figure 4c. The first component ($\tau_1 = 530$ fs) corresponds to the initial sub-picosecond spectral evolution, with a negative feature at 700–750 nm representing the grow-in of the $2^1A_g \leftarrow 1^1B_{3u}$ ESA signal and a broad but low-intensity positive feature from 500–700 nm. This first component arises from direct excitation of the perylene 2^1B_{2u} state and converts into the 1^1B_{3u} state (evidenced by the $2^1A_g \leftarrow 1^1B_{3u}$ ESA growth) and is therefore assigned as $2^1B_{2u} \rightarrow 1^1B_{3u}$ IC. The EADS of the second component ($\tau_2 = 23.9$ ps) exhibits ESA signals from 600–850 nm, similar to those observed upon 440-nm excitation of

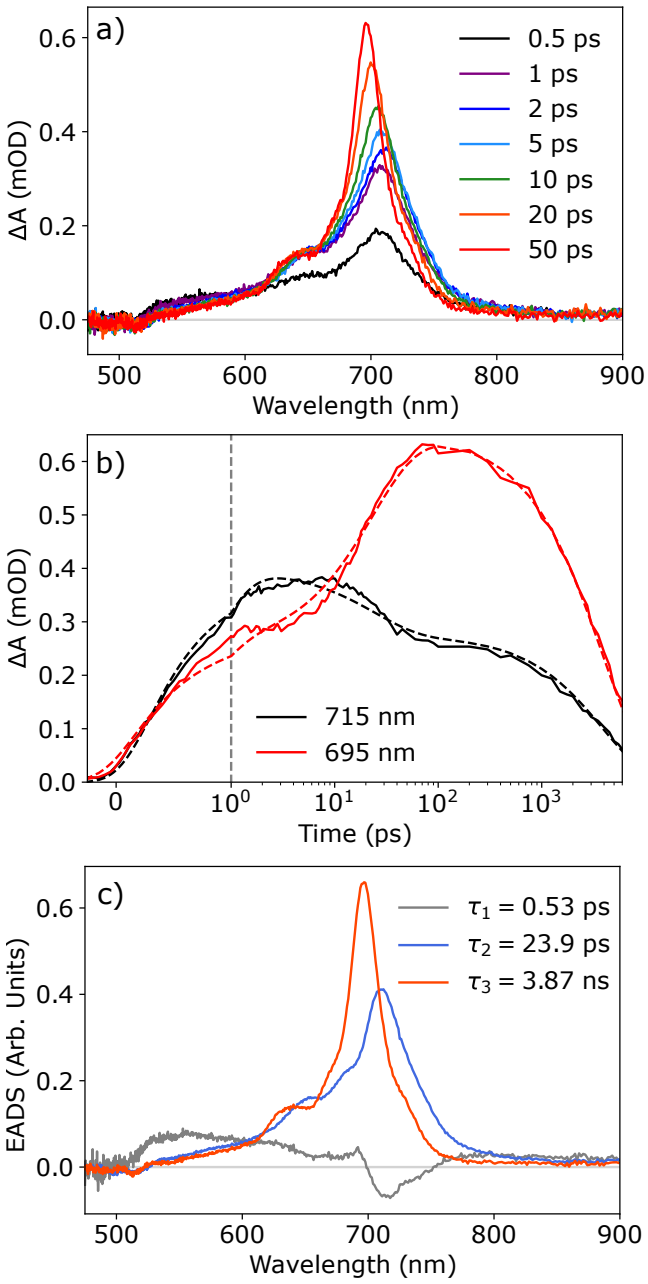

Figure 4: (a) Transient absorption spectra of 100 µM perylene/cyclohexane upon excitation at 270 nm. (b) Single-wavelength kinetic traces of the ESA transient features at 695 and 715 nm (solid curves) and fits at these wavelengths from global analysis (dashed curves). (c) Evolution-associated difference spectra (EADS) extracted from a global fit to the TA data with a 3-component sequential kinetic model. EADS are labelled by their characteristic time constants τ_i.

perylene but significantly broadened and redshifted. This EADS resembles the broadened and redshifted ΔA signal attributed above to the formation of a vibrationally-hot 1^1B_{3u} state following $2^1A_g \rightarrow 1^1B_{3u}$ IC (Figure 3a). It is therefore reasonable to infer that these transient spectra arise from similar physical processes, and so we assign the second component here as a vibrationally-excited 1^1B_{3u} state formed from $2^1B_{2u} \rightarrow 1^1B_{3u}$ IC. Finally, the third EADS ($\tau_3 = 3.87\,\text{ns}$) is identical to the transient spectrum of perylene upon 440 nm excitation shown in Figure 2, and clearly corresponds to relaxation of the 1^1B_{3u} state.

A similar 3-component model was recently used by Ni et al. to describe the ultrafast dynamics of perylene upon 250-nm excitation;[29] however they report a time constant for $2^1B_{2u} \rightarrow 1^1B_{3u}$ IC of 900 fs, which disagrees with the value measured here by almost a factor of two. The authors of that particular work noted that their pump and probe beams were polarised parallel to one another rather than at the magic angle, and so their results may also contain contributions from the rotational dynamics of perylene. Repetition of experiments here with pump-probe polarisation set to parallel rather than the magic angle was able to reproduce this result, with an apparent IC time constant of 950 fs at parallel pump-probe polarisation (Supporting Information, Section S6). The $1^1B_{3u} \leftarrow 1^1A_g$ and $2^1B_{2u} \leftarrow 1^1A_g$ transitions in perylene are known to have transition dipole moments perpendicular to one another,[46] and so based upon the polarisation-dependent results presented in Figure 2, the $2^1B_{2u} \leftarrow 1^1A_g$ and $2^1A_g \leftarrow 1^1B_{3u}$ transition dipole moments must therefore also be perpendicular to each other. Sub-picosecond $2^1B_{2u} \rightarrow 1^1B_{3u}$ IC hence prepares perylene molecules with the $2^1A_g \leftarrow 1^1B_{3u}$ transition dipole moment polarised perpendicular to the pump pulse, and so at parallel pump-probe polarisation the observed transient signal will be convoluted with the dynamics of molecules rotating into the plane of polarisation. This therefore illustrates the importance of ensuring magic-angle pump-probe polarisation when using transient absorption techniques to measure ultrafast exciton dynamics, as molecular rotational dynamics can occur on similar timescales to excitonic processes and thus complicate the interpretation of time-resolved data.

The excited-state processes of perylene studied in this work are summarized in Figure 1. Five electronic excited states are accessible through UV-visible excitation: the 1^1B_{3u}, 1^1B_{2u} and 2^1B_{2u} states through single-photon absorption, as well as the 2^1A_g and 3^1A_g states through sequential two-photon excitation via the 1^1B_{3u} state. Excitation to either the 2^1A_g or 2^1B_{2u} states results in sub-picosecond IC to the lower-energy 1^1B_{3u} state. In molecular systems with relatively weak vibronic couplings, the rates of radiationless electronic transitions such as IC are expected to follow the "Energy-Gap Law":

$$k_{\mathrm{IC}} \propto \exp\left(-\frac{\Delta E}{k_{\mathrm{B}}T}\right), \tag{3}$$

where ΔE is the energy gap between electronic states, k_{B} is the Boltzmann constant and T is temperature.[47,48] We assume $\Delta E_{2A_g-1B_{3u}}$ to be equivalent to the $2^1A_g \leftarrow 1^1B_{3u}$ transition energy observed here (695 nm; 1.78 eV), and estimate $\Delta E_{2B_{2u}-1B_{3u}}$ as approximately 2.15 eV from Figure 1. Using these values, Equation 3 predicts that $2^1A_g \rightarrow 1^1B_{3u}$ IC in perylene will occur at a rate 1.46× faster than $2^1B_{2u} \rightarrow 1^1B_{3u}$ IC, in reasonable agreement with the IC rates measured here (1.56× faster from the 2^1A_g state). To the best of our knowledge, this is the first reported measurement of $2^1A_g \rightarrow 1^1B_{3u}$ relaxation in perylene, and revises the rate of $2^1B_{2u} \rightarrow 1^1B_{3u}$ IC previously reported by Ni et al.[29]

It is worth noting that these IC processes could proceed either directly from the initially excited states to the 1^1B_{3u} state, or indirectly via other close-lying electronic excited states. IC is quantified here by observing the recovery of the 1^1B_{3u} state, and so these experiments cannot distinguish between direct and indirect relaxation pathways. To estimate the contributions of direct and indirect IC processes here, we calculate electronic-nuclear couplings between all singlet excited states of interest (Supporting Information, Section S7). For both the 2^1B_{2u} and 2^1A_g states of perylene, significant couplings are observed to the 1^1B_{3u} state and other singlet excited states, while couplings to the ground (1^1A_g) state are effectively negligible. These results therefore suggest that multiple IC pathways may exist for both of

these high-lying excited states, and so repopulation of the 1^1B_{3u} state could occur simultaneously through both direct and indirect IC processes. The IC time constants quantified here therefore likely represent weighted averages across all possible relaxation pathways from the initially-populated higher excited states.

Upon populating the 1^1B_{3u} state through IC from either high-lying electronic state, vibrational cooling via solvent-solute VET occurs on a timescale of tens of picoseconds. This is of a similar order of magnitude to previous measurements of VET for perylene in hexane solution,[41,44] although the exact rates differ due to the varying quantities of excess vibrational energy deposited into the 1^1B_{3u} manifold through each process. We note that the rate of VET measured here is slightly faster following $2^1A_g \rightarrow 1^1B_{3u}$ IC when compared to $2^1B_{2u} \rightarrow 1^1B_{3u}$ relaxation, presumably due to the latter process depositing a greater amount of excess vibrational energy into the lower electronic state.

Triplet formation through SF was not observed under any of the excitation conditions used here, as these experiments were undertaken in dilute solution so as to isolate the ultrafast dynamics of perylene's higher electronic excited states. SF in condensed-phase perylene has been reported to occur within 50 fs when excited at sufficiently high energy; however, there has been some disagreement as to whether SF in perylene occurs directly from the 2^1B_{2u} state or a vibrationally-hot 1^1B_{3u} state following IC.[23,26,27] We note that the reported rate of SF is over an order of magnitude faster than that of $2^1B_{2u} \rightarrow 1^1B_{3u}$ IC measured here, which would suggest some significant level of SF must proceed directly from this higher electronic excited state. However, other studies have demonstrated that triplet excitons are also observed upon excitation of a higher vibronic band of the $1^1B_{3u} \leftarrow 1^1A_g$ transition,[23,24] and so some SF must also occur from a vibrationally-hot 1^1B_{3u} state. It is therefore likely that in perylene both of these SF pathways occur in parallel, as was recently proposed by Bai et al for SF in rubrene.[28]

Interestingly, the SF rate reported for crystalline perylene is also significantly faster than the rate of relaxation from the 2^1A_g state observed here. It may therefore also be possible

for SF to proceed from this optically dark state, provided that sufficient electronic coupling exists between the 2^1A_g and ^{1}(TT) states. As we believe the present work to be the first spectroscopic study of the perylene 2^1A_g state, the potential for SF to occur from this state in the condensed phase has not previously been examined. As the 2^1A_g state is only accessible from the ground state through two-photon excitation, SF from this high-lying state could be extremely useful in developing ultrafast molecular logic devices. Populating the 2^1A_g state would require sequential $2^1A_g \leftarrow 1^1B_{3u} \leftarrow 1^1A_g$ excitation at two spectrally-distinct wavelengths, and so SF from this state could only occur in the presence of both inputs (analogous to a logical AND operation). Triplet excitons exhibit very distinctive magneto-optical properties while singlets are insensitive to magnetic fields,[49] and so triplet detection through magnetometry would allow for cleanly distinguishing between "on" and "off" states. The sub-picosecond timescale on which SF occurs from perylene's higher excited states would also enable signal processing to occur orders of magnitude faster than molecular logic devices employing photoswitchable chromophores.[8,9] Harnessing SF from perylene's high-lying electronic excited states may therefore hold significant potential for developing ultrafast "excitonic" logical devices, and we hope to explore this further in a future work.

In summary, this study used femtosecond transient absorption spectroscopy to identify high-lying electronic excited states of perylene and quantify their relaxation dynamics in cyclohexane solution. A strong excited-state absorption is evident upon excitation to the low-lying 1^1B_{3u} state, which by polarisation-dependent measurements was identified as the $2^1A_g \leftarrow 1^1B_{3u}$ transition. Population of the 2^1A_g state by sequential pump-push excitation resulted in $2^1A_g \rightarrow 1^1B_{3u}$ internal conversion with a time constant of 340 fs, with subsequent vibrational cooling of the 1^1B_{3u} state over tens of picoseconds. The perylene 2^1B_{2u} state is accessible directly from the ground state by UV excitation, and a lifetime of 530 fs is recorded for this higher excited state. The rates of internal conversion from these two higher-excited states measured here are consistent with the energy gap law, and are both an order of magnitude slower than reported rates of SF in perylene. This therefore suggests that SF

in perylene may be achievable through sequential two-colour excitation to the 2^1A_g state, which may be highly beneficial in the development of ultrafast molecular logic devices.

Supporting Information Available

Experimental and computational methods; additional computational results; additional pump-probe data; push-probe control experiments; solvent-dependence of pump-push-probe kinetics; UV pump-probe results at parallel polarisation; estimating inter-excited-state couplings in perylene.

Acknowledgements

This work was supported by the Australian Research Council (ARC) Centre of Excellence in Exciton Science (CE170100026) and the ARC Linkage Infrastructure, Equipment and Facilities Scheme (LE200100051). This work was also supported by computational resources provided by the Australian Government through the National Computational Infrastructure National Facility and the Pawsay Supercomputer Centre. RJH would also like to thank Dr. Nina Novikova for technical support.

References

(1) Andréasson, J.; Pischel, U. Light-Stimulated Molecular and Supramolecular Systems for Information Processing and Beyond. *Coord. Chem. Rev.* **2021**, *429*, 213695.

(2) Erbas-Cakmak, S.; Kolemen, S.; Sedgwick, A. C.; Gunnlaugsson, T.; James, T. D.; Yoon, J.; Akkaya, E. U. Molecular Logic Gates: The Past, Present and Future. *Chem. Soc. Rev.* **2018**, *47*, 2228–2248.

(3) Aviram, A. Molecules for Memory, Logic, and Amplification. *J. Am. Chem. Soc.* **1988**, *110*, 5687–5692.

(4) Balzani, V.; Credi, A.; Raymo, F. M.; Stoddart, J. F. Artificial Molecular Machines. *Angew. Chem. Int. Ed.* **2000**, *39*, 3348–3391.

(5) de Silva, P. A.; Gunaratne, N. H. Q.; McCoy, C. P. A Molecular Photoionic AND Gate Based on Fluorescent Signalling. *Nature* **1993**, *364*, 42–44.

(6) Margulies, D.; Melman, G.; Felder, C. E.; Arad-Yellin, R.; Shanzer, A. Chemical Input Multiplicity Facilitates Arithmetical Processing. *J. Am. Chem. Soc.* **2004**, *126*, 15400–15401.

(7) Margulies, D.; Melman, G.; Shanzer, A. Fluorescein as a Model Molecular Calculator with Reset Capability. *Nat. Mater.* **2005**, *4*, 768–771.

(8) Andréasson, J.; Straight, S. D.; Moore, T. A.; Moore, A. L.; Gust, D. Molecular All-Photonic Encoder-Decoder. *J. Am. Chem. Soc.* **2008**, *130*, 11122–11128.

(9) Andréasson, J.; Pischel, U.; Straight, S. D.; Moore, T. A.; Moore, A. L.; Gust, D. All-Photonic Multifunctional Molecular Logic Device. *J. Am. Chem. Soc.* **2011**, *133*, 11641–11648.

(10) Budyka, M. F.; Li, V. M. Multifunctional Photonic Molecular Logic Gate Based On A Biphotochromic Dyad With Reduced Energy Transfer. *ChemPhysChem* **2017**, *18*, 260–264.

(11) Remacle, F.; Speiser, S.; Levine, R. D. Intermolecular and Intramolecular Logic Gates. *J. Phys. Chem. B* **2001**, *105*, 5589–5591.

(12) Sawaya, N. P. D.; Rappoport, D.; Tabor, D. P.; Aspuru-Guzik, A. Excitonics: A Set of Gates for Molecular Exciton Processing and Signaling. *ACS Nano* **2018**, *12*, 6410–6420.

(13) Kasha, M. Characterization of Electronic Transitions in Complex Molecules. *Disc. Faraday Soc.* **1950**, *9*, 14–19.

(14) Beer, M.; Longuet-Higgins, H. C. Anomalous Light Emission of Azulene. *J. Chem. Phys.* **1955**, *23*, 1390–1391.

(15) Viswanath, G.; Kasha, M. Confirmation of the Anomalous Fluorescence of Azulene. *J. Chem. Phys.* **1956**, *24*, 574–577.

(16) Wagner, B. D.; Tittelbach-Helmrich, D.; Steer, R. P. Radiationless Decay of the S2 States of Azulene and Related Compounds: Solvent Dependence and the Energy Gap Law. *J. Phys. Chem.* **1992**, *96*, 7904–7908.

(17) Kuznetz, O.; Davis, D.; Salman, H.; Eichen, Y.; Speiser, S. Intramolecular Electronic Energy Transfer in Rhodamine-Azulene Bichromophoric Molecule. *J. Photochem. Photobiol. A* **2007**, *191*, 176–181.

(18) Kuznetz, O.; Salman, H.; Eichen, Y.; Remacle, F.; Levine, R. D.; Speiser, S. All Optical Full Adder Based on Intramolecular Electronic Energy Transfer in the Rhodamine-Azulene Bichromophoric System. *J. Phys. Chem. C* **2008**, *112*, 15880–15885.

(19) Tittelbach-Helmrich, D.; Wagner, B. D.; Steer, R. P. Subpicosecond Vibrational Relaxation of the S_1 States of Azulene and Guaiazulene in Solution. *Can. J. Chem.* **1995**, *73*, 303–306.

(20) Bearpark, M. J.; Bernardi, F.; Clifford, S.; Olivucci, M.; Robb, M. A.; Smith, B. R.; Vreven, T. The Azulene S_1 State Decays via a Conical Intersection: A CASSCF Study with MMVB Dynamics. *J. Am. Chem. Soc.* **1996**, *118*, 169–175.

(21) Steer, R. P. Photophysics of Molecules Containing Multiples of the Azulene Carbon Framework. *J. Photochem. Photobiol. C Photochem. Rev.* **2019**, *40*, 68–80.

(22) Ma, L.; Tan, K. J.; Jiang, H.; Kloc, C.; Michel-Beyerle, M.-E.; Gurzadyan, G. G. Excited-State Dynamics in an α-Perylene Single Crystal: Two-Photon- and Consecutive Two-Quantum-Induced Singlet Fission. *J. Phys. Chem. A* **2014**, *118*, 838–843.

(23) Ni, W.; Sun, L.; Gurzadyan, G. G. Ultrafast Spectroscopy Reveals Singlet Fission, Ionization and Excimer Formation in Perylene Film. *Sci. Rep.* **2021**, *11*, 5220.

(24) Albrecht, W. G.; Michel-Beyerle, M. E.; Yakhot, V. Exciton Fission in Excimer Forming Crystal. Dynamics of an Excimer Build-Up in α-Perylene. *Chem. Phys.* **1978**, *35*, 193–200.

(25) Sun, S.; Conrad-Burton, F. S.; Liu, Y.; Ng, F.; Steigerwald, M.; Zhu, X.; Nuckolls, C. Inducing Singlet Fission in Perylene Thin Films by Molecular Contortion. *J. Phys. Chem. A* **2022**, *126*, 7559–7565.

(26) Ni, W.; Gurzadyan, G. G.; Zhao, J.; Che, Y.; Li, X.; Sun, L. Singlet Fission from Upper Excited Electronic States of Cofacial Perylene Dimer. *J. Phys. Chem. Lett.* **2019**, *10*, 2428–2433.

(27) Zhang, Z.; Ni, W.; Ma, L.; Sun, L.; Gurzadyan, G. G. Enhancement of Singlet Fission Yield by Hindering Excimer Formation in Perylene Film. *J. Phys. Chem. C* **2022**, *126*, 396–403.

(28) Bai, Y.; Ni, W.; Sun, K.; Chen, L.; Ma, L.; Zhao, Y.; Gurzadyan, G. G.; Gelin, M. F. Plenty of Room on the Top: Pathways and Spectroscopic Signatures of Singlet Fission from Upper Singlet States. *J. Phys. Chem. Lett.* **2022**, 11086–11094.

(29) Ni, W.; Gurzadyan, G. G.; Sun, L.; Gelin, M. F. Toward Efficient Photochemistry from Upper Excited Electronic States: Detection of Long S2 Lifetime of Perylene. *J. Chem. Phys.* **2021**, *155*, 191102.

(30) Gudipati, M. S. Exciton, Exchange, and Through-Bond Interactions in Multichromophoric Molecules: An Analysis of the Electronic Excited States. *J. Phys. Chem.* **1994**, *98*, 9750–9763.

(31) Manian, A.; Hudson, R. J.; Ramkissoon, P.; Smith, T. A.; Russo, S. P. Interexcited State Photophysics I: Benchmarking Density Functionals for Computing Nonadiabatic Couplings and Internal Conversion Rate Constants. *J. Chem. Theory Comput.* **2022**, *19*, 271–292.

(32) Olmsted, J. Calorimetric Determinations of Absolute Fluorescence Quantum Yields. *J. Phys. Chem.* **1979**, *83*, 2581–2584.

(33) Taniguchi, M.; Lindsey, J. S. Database of Absorption and Fluorescence Spectra of >300 Common Compounds for use in PhotochemCAD. *Photochem. Photobiol.* **2018**, *94*, 290–327.

(34) Shibasaki, Y.; Suenobu, T.; Nakagawa, T.; Katoh, R. Effect of Deuteration on Relaxation Dynamics of the Perylene Excimer Studied by Subnanosecond Transient Absorption Spectroscopy. *J. Phys. Chem. A* **2021**, *125*, 1359–1366.

(35) Karabunarliev, S.; Baumgarten, M.; Müllen, K. Crossover to an Even-Parity Lowest Excited Singlet in Large Oligorylenes: A Theoretical Study. *J. Phys. Chem. A* **1998**, *102*, 7029–7034.

(36) Tanizaki, Y.; Yoshinaga, T.; Hiratsuka, H. Assignment of Electronic Spectrum of Perylene. *Spectrochim. Acta A Mol. Spectrosc.* **1978**, *34*, 205–210.

(37) Casanova, D. Theoretical Investigations of the Perylene Electronic Structure: Monomer, Dimers, and Excimers. *Int. J. Quantum Chem.* **2015**, *115*, 442–452.

(38) Kiba, T.; Sato, S.-i.; Akimoto, S.; Kasajima, T.; Yamazaki, I. Solvent-Assisted In-

tramolecular Vibrational Energy Redistribution of S_1 Perylene in Ketone Solvents. *J. Photochem. Photobiol. A* **2006**, *178*, 201–207.

(39) Pigliucci, A.; Duvanel, G.; Daku, L. M. L.; Vauthey, E. Investigation of the Influence of Solute-Solvent Interactions on the Vibrational Energy Relaxation Dynamics of Large Molecules in Liquids. *J. Phys. Chem. A* **2007**, *111*, 6135–6145.

(40) Jiang, Y.; Blanchard, G. J. Rotational Diffusion Dynamics of Perylene in n-Alkanes. Observation of a Solvent Length-Dependent Change of Boundary Condition. *J. Phys. Chem.* **1994**, *98*, 6436–6440.

(41) Qiu, C.; Blanchard, G. J. Orientational and Vibrational Relaxation Dynamics of Perylene in the Cyclohexane-Ethanol Binary Solvent System. *J. Phys. Chem. B* **2014**, *118*, 10525–10533.

(42) Graener, H.; Seifert, G.; Laubereau, A. Direct Observation of Rotational Relaxation Times by Time-Resolved Infrared Spectroscopy. *Chem. Phys. Lett.* **1990**, *172*, 435–439.

(43) Lin, Y.-S.; Pieniazek, P. A.; Yang, M.; Skinner, J. L. On the Calculation of Rotational Anisotropy Decay, as Measured by Ultrafast Polarization-Resolved Vibrational Pump-Probe Experiments. *J. Chem. Phys.* **2010**, *132*, 174505.

(44) Jiang, Y.; Blanchard, G. Vibrational Population Relaxation of Perylene in n-Alkanes. The Role of Solvent Local Structure in Long-Range Vibrational Energy Transfer. *J. Phys. Chem.* **1994**, *98*, 9411–9416.

(45) Snellenburg, J. J.; Laptenok, S.; Seger, R.; Mullen, K. M.; van Stokkum, I. H. M. Glotaran: A Java-Based Graphical User Interface for the R Package TIMP. *J. Stat. Soft.* **2012**, *49*, 1 – 22.

(46) Thulstrup, E. W.; Michl, J.; Eggers, J. Polarization Spectra in Stretched Polymer

Sheets. II. Separation of π–π Absorption of Symmetrical Molecules into Components. *J. Phys. Chem.* **1970**, *74*, 3868–3878.

(47) Englman, R.; Jortner, J. The Energy Gap Law for Radiationless Transitions in Large Molecules. *Mol. Phys.* **1970**, *18*, 145–164.

(48) Englman, R.; Jortner, J. The Energy Gap Law for Non-Radiative Decay in Large Molecules. *J. Lumin.* **1970**, *1-2*, 134–142.

(49) Xu, R.; Zhang, C.; Xiao, M. Magnetic Field Effects on Singlet Fission Dynamics. *Trends Chem.* **2022**, *4*, 528–539.